ACS EARTH AND SPACE CHEMISTRY

http://pubs.acs.org/journal/aesccq

Article

Probing Heterogeneous Efflorescence of Mars-Relevant Salts with an Optical Levitator

Shuichi B. Ushijima, Raina V. Gough, and Margaret A. Tolbert*

Cite This: *ACS Earth Space Chem.* 2020, 4, 1947−1956

Read Online

ACCESS | Metrics & More | Article Recommendations | Supporting Information

ABSTRACT: The presence of liquid water on the surface and subsurface of Mars has been of interest because liquid water is essential for life as we know it. While pure liquid water is typically not stable on present-day Mars, brines of hygroscopic salts with low eutectic temperatures could be stable during certain periods of a Martian sol. Studies on these salts have focused on their homogeneous phase transitions, but the impact that Martian soil may have on the brine stability is not well established. Here, using optical levitation, we examined heterogeneous efflorescence of $Mg(ClO_4)_2$ induced by contact with a crystal of itself, NaCl, $(NH_4)_2SO_4$, montmorillonite, and Mojave Mars Simulant (MMS) at room temperature. NaCl and $(NH_4)_2SO_4$ were chosen to analyze the effect of crystal lattice on heterogeneous efflorescence. In addition, contact efflorescence of $Ca(ClO_4)_2$ and $CaCl_2$ by montmorillonite was studied. The stability of all three brines was unaffected by contact with montmorillonite. An immersed heterogeneous particle can also induce efflorescence from within a droplet. The effect of immersed montmorillonite was probed for all three brines plus $MgCl_2$, and the effect of immersed MMS was probed for $Mg(ClO_4)_2$. The immersed particles of montmorillonite increased the efflorescence relative humidity of $MgCl_2$ but did not affect the other brines. The inactivity of montmorillonite as a heterogeneous nucleus supports the possibility of brine stability on Mars because even salt particles in contact with or coating soil grains may sustain a brine without interference from the soil.

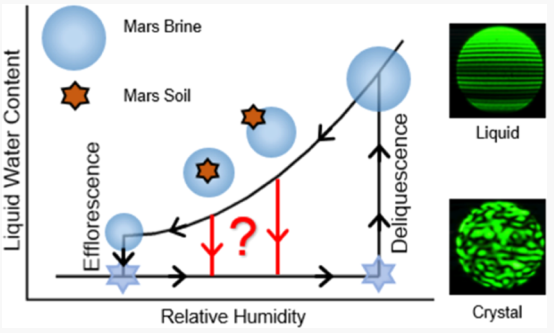

KEYWORDS: *contact efflorescence, immersion efflorescence, Mars, brines, crystal lattice, water*

1. INTRODUCTION

Liquid water is currently the only biochemical solvent that is known to be used by life[1] and thus has been a factor in determining the habitability of planets.[1,2] Mars is widely believed to have had liquid water in its ancient past based on geomorphological features and the presence of clay minerals.[3−6] While water ice and water vapor have been observed and measured, on current Mars, the instability of liquid water at low Martian pressures has made its detection challenging. Although pure liquid water may be unstable, it has been hypothesized that liquid water may be present in the form of a brine.[7−19] Landers on the surface and satellites orbiting Mars have shown that inorganic salts, such as perchlorates and chlorides, are present in the Martian regolith and are believed to be found globally.[20−23] Some of these salts are highly hygroscopic and can deliquesce to form briny solutions at low relative humidities (RHs). Recently, the Mars Advanced Radar for Subsurface and Ionosphere Sounding (MARSIS) has detected a subglacial pond, which could potentially be composed of brine.[24] Additionally, hydrates of salts that could potentially form brine may have been detected near recurring slope lineae (RSL) by the Compact Reconnaissance Imaging Spectrometer for Mars (CRISM).[8] RSL are geographic features that are characterized by dark streaks that slowly grow on steep slopes seasonally. The formation mechanism has yet to be determined but brines have been considered as potentially having a role in RSL behavior.[8,9,15] To fully understand the role of brines on present-day Mars, it is essential to detail how salts interact with water under Martian conditions including the presence of minerals composing the regolith.

The salt and water stability diagram includes three general phases: brine ice, liquid brine, and crystalline salt, possibly hydrated. Here, we focus on the transitions between the liquid brine and the crystalline phase. The crystalline salt will absorb water vapor from the surrounding environment and transition into a brine, i.e., deliquesce, at a specific relative humidity termed the deliquescence relative humidity (DRH). The reverse process, efflorescence, usually occurs at a distinctly lower efflorescence relative humidity (ERH). The hysteresis between the DRH and the ERH is due to a nucleation barrier

Received: June 17, 2020
Revised: September 17, 2020
Accepted: September 23, 2020
Published: September 23, 2020

https://dx.doi.org/10.1021/acsearthspacechem.0c00161
ACS Earth Space Chem. 2020, 4, 1947−1956

that kinetically hinders homogeneous efflorescence. The hysteresis effect allows the brine to exhibit metastable supersaturation when the RH conditions fall below the DRH. Laboratory studies on the phase transitions of salts believed to be on the surface of Mars have been conducted at Mars-relevant temperatures and RH using a droplet on a plate technique.[10−14,16,17] When the results are compared to modeled results of temperature and RH at the surface of Mars, it is concluded that brines could be stable or metastable during certain times of a Martian year and sol.[10−15] In the subsurface where temperature conditions are more suitable for brine stability, brines could be present for much longer.[13] Additionally, a study on bulk samples of Mars-relevant salts also showed their supercooling capabilities, further supporting brine stability on Mars' surface and subsurface.[18,19] However, on the surface and subsurface, the brines will inevitably interact with the Martian regolith, where soil particles could act as heterogeneous nuclei and potentially induce efflorescence of a brine at a higher humidity than the homogeneous ERH.

In heterogeneous nucleation, the presence of a foreign nucleus can lower the energy barrier needed for a crystal seed to form, thus aiding the crystallization process. For heterogeneous efflorescence, the effect manifests as a decrease in the metastability of the brine through the increase in the ERH. Heterogeneous efflorescence occurs via two distinct pathways, immersion mode and contact mode. During immersion efflorescence, the heterogeneous nucleus induces crystallization from within the droplet. Contact efflorescence occurs when the nucleus interacts with the surface and induces crystallization from the outside. On Mars, immersion mode efflorescence could affect all brines that form on the surface or in the subsurface when salts and minerals are internally mixed. Contact efflorescence could occur near the surface of Mars where dust fall is common and at the liquid front of a flowing brine at the surface or subsurface. Laboratory studies performed on heterogeneous efflorescence[17,25−30] show that the effect of a heterogeneous nucleus on efflorescence varies greatly based on the brine and nucleus pair. Some pairs, such as magnesium perchlorate ($Mg(ClO_4)_2$) and montmorillonite, show minimal to no effect on the brine stability[17] when droplets on a plate are investigated. In contrast, other pairs, such as sodium chloride (NaCl) and montmorillonite, result in a significant decrease in brine stability.[27] Studies with immersed particles of heterogeneous nuclei have also shown that the effect on brine-freezing temperature varies with brine and nucleus pair.[17,18,31] Unfortunately, no comprehensive model that can explain the various results exists and thus we must rely on laboratory experiments. An additional observation that has yet to be explained theoretically is the observation that the same nucleus can be more effective in contact nucleation than immersion nucleation.[27,32] The higher efficiency of contact nucleation may disproportionately affect brines near the Martian surface, making the exposed surface less ideal for brine metastability than previously believed. Here, we use a novel optical levitation experiment to probe the effect of heterogeneous efflorescence on four Mars-relevant salts by a series of heterogeneous nuclei.

2. BACKGROUND AND CHOICE OF SYSTEM FOR STUDY

The Martian regolith has been characterized remotely and at the surface through various techniques such as infrared spectroscopy, mass spectrometry, gas chromatography, and X-ray diffraction (XRD).[4−6,33−36] The upper layer of the Martian crust is mostly basaltic rock, composed of various mineral groups such as olivines, plagioclase feldspar, orthopyroxenes, and silicate glasses. Depending on the region, the actual composition of the basaltic crust can vary. For example, the southern highlands have a higher proportion of plagioclase, while the northern plains have more silicate phases.[33] In addition to the basaltic species, other secondary species, such as phyllosilicates or clay minerals, sulfates, and oxides, have been measured in localized regions. For example, clay minerals have been observed at Gale Crater where Mars' earliest terrain has become exposed.[5,36] These clay minerals are believed to have formed early in Mars' history during which nonacidic aqueous environments interacted with the basaltic crust to alter their mineralogy.[4,36] In their paper from 2006, Bibring et al.[4] termed it the phyllosian period to indicate the formation of clay minerals during this time. It is unclear how these different minerals may impact the stability of brines on current Mars. To examine the effect of mineral particles on efflorescence, two mineral samples were chosen as heterogeneous nuclei in our experiments: montmorillonite and Mojave Mars Simulant (MMS). Montmorillonite is a clay mineral, while MMS is a Mars soil analogue that is collected from crushing basaltic boulders from the Mojave Desert.[37] Montmorillonite belongs to the smectite group, which has been detected on the surface of Mars,[6,36] and MMS has similar chemical and physical characteristics to Mars dust.[37]

The stability of brines for four salts that are believed to be present on the surface and in the subsurface of Mars was investigated using the optical levitator. The four brines were $Mg(ClO_4)_2$, magnesium chloride ($MgCl_2$), calcium perchlorate ($Ca(ClO_4)_2$), and calcium chloride ($CaCl_2$). These four salts were chosen due to the actual detection of the salt itself or the individual ions having been detected in the Martian soil.[8,20,21,38] Perchlorate anion has been found by both the Wet Chemistry Laboratory aboard the Phoenix lander and the Sample Analysis at Mars instrument aboard the Curiosity Rover at Gale Crater.[20,21] The Phoenix lander also measured cations and found magnesium and sodium to be the dominant species and calcium was detected at lower concentrations.[20] The Thermal Emission Imaging System (THEMIS) aboard the Mars Odyssey orbiter has detected signals that are believed to be from chloride-bearing materials.[38]

Contact efflorescence of aqueous $Mg(ClO_4)_2$ by crystalline $Mg(ClO_4)_2$, NaCl, and ammonium sulfate ($(NH_4)_2SO_4$) was first investigated. As these salts are soluble, immersion efflorescence was not possible and thus was not investigated. The crystal of $Mg(ClO_4)_2$ was chosen because it should act as a perfect crystal seed and be highly efficient at inducing heterogeneous nucleation. Past studies using the optical levitator have shown that seeded crystal growth will occur at RH values very near the DRH, effectively shutting down hysteresis and the potential for supersaturated brines.[25,26] On Mars, the interaction between a brine and crystal of the same salt could occur if crystals from a dryer region were carried by wind to an area where its brine had formed. NaCl, which is also expected to be found on Mars,[20,38] was chosen because it maintains its crystalline structure at higher RH values and has a different crystal lattice structure and shape. While $(NH_4)_2SO_4$ is not thought to be a constituent of the Martian surface, it was chosen because it has a more similar crystalline structure to $Mg(ClO_4)_2$ than does NaCl. The effect of crystal structure on heterogeneous efflorescence will be analyzed based on the

https://dx.doi.org/10.1021/acsearthspacechem.0c00161
ACS Earth Space Chem. 2020, 4, 1947−1956

crystal lattice constants of the heterogeneous nuclei. In addition to the soluble heterogeneous nuclei, $Mg(ClO_4)_2$ was exposed to montmorillonite and MMS to observe the effect of the insoluble heterogeneous nuclei in both contact and immersion efflorescence. For $MgCl_2$, only immersion efflorescence by montmorillonite was investigated as the contact ERH of $MgCl_2$ by montmorillonite has already been examined and reported in a previous study using the optical levitator.[27] Finally, contact and immersion efflorescence of the two remaining brines of $Ca(ClO_4)_2$ and $CaCl_2$ by montmorillonite were investigated.

3. EXPERIMENTAL SETUP

3.1. Optical Levitation and Flow Cell Arrangement. The optical levitator used in this study has been described in detail previously[25] and thus will only be briefly discussed here. Droplets of aqueous salts are trapped by two vertical counterpropagating laser beams from a 532 nm Nd:YAG source that has been split in half. The two beams enter a closed flow cell with multiple windows for observation. The beam entering the flow cell from below has a Gaussian profile, while the beam from above has a Bessel profile. The laser beams exert a scattering force in the direction of the laser propagation. In addition, a gradient force toward higher intensity moves the particle toward the center of the beam. The scattering forces from the two counterpropagating lasers, the force of gravity, and the drag force from air flowing up through the flow cell balance out in the vertical direction. The gradient forces of the lasers stabilize the trap by keeping the trapped particle on axis.

The air flowing through the cell consists of two streams of pure nitrogen gas controlled with mass flow controllers. The first stream flows through a bubbler containing HPLC-grade water to humidify the flow. The second stream flows through a diffusion drier and is then mixed with the humidified nitrogen prior to entering the cell. By adjusting the amounts of humidified and dry flows, the RH inside the flow cell is controlled. RH and temperature are measured by individual probes (Vaisala HMP 60) at the inlet and outlet of the cell. The RH inside the flow cell is calculated as the average of the two probes (±1 S.D.).

To create heterogeneous nuclei, the dry flow is diverted toward a nebulizer (Omron NE-U22) filled with 3−4 mL of an aqueous solution or a suspension of mineral particles in water. The nebulizer creates a mist that is carried by the nitrogen gas into the diffusion drier to remove the water, forming heterogeneous nuclei of salt crystals or mineral particles. The gas carrying the heterogeneous nuclei mixes with the humidified flow and enters the flow cell where the nuclei interact with the trapped droplet. Forming heterogeneous nuclei of insoluble minerals from a mixture in water and drying have the potential to change the surface properties of the mineral particle due to a redistribution of the soluble portion of the mineral during the wetting.[39] However, the effect of any change in mineral surface properties on the heterogeneous efflorescence efficiency has not been studied. Further, minerals on Mars may have experienced such aging processes during their lifetime as they interact with brines or ice.

To manipulate the heterogeneous nuclei, the flow cell is attached to a slidable stage with mobility in both horizontal directions. The movable flow cell allows us to control where the heterogeneous nuclei flow relative to the position of the trapped droplet. The optics, such as mirrors and lenses, that guide the laser into the flow cell are not moved and thus the trapped droplet does not move. However, by moving the flow cell, the particle stream of heterogeneous nuclei can be adjusted to be aligned or misaligned with the lasers. When the particle stream is misaligned, no collisions between heterogeneous nuclei and droplet occur and when aligned collisions occur.

3.2. Generating Droplets of Aqueous Solution. A droplet generator (Microfab MJ-APB-20) was used to produce droplets of aqueous solutions to be trapped. For droplet generation, solutions of 5 wt % $Mg(ClO_4)_2$ (Sigma-Aldrich), $MgCl_2$ (Mallinckrodt), $Ca(ClO_4)_2$ (Sigma-Aldrich), and $CaCl_2$ (Fisher Scientific) were first filtered through a 0.22 μm pore nylon filter. The droplet generator was then filled with the solution and inserted into a side port near the top of the flow cell. The tip of the droplet generator is made of a glass capillary with a 20 μm orifice. An alternating positive and negative voltage on a ring made of a piezoelectric material near the tip of the glass capillary pushes droplets out into the flow cell to be caught by the lasers. After equilibration, the typical size of the trapped droplet is 10−15 μm in diameter.

3.3. Generating Contact Nuclei. For generation of soluble heterogeneous nuclei, aqueous solutions of 10 wt % $Mg(ClO_4)_2$, NaCl (Mallinckrodt), and $(NH_4)_2SO_4$ (Sigma-Aldrich) in HPLC-grade water were prepared. For nonsoluble mineral particles, montmorillonite (SWy-2b) was obtained from the Clay Mineral Society and MMS was obtained from the Jet Propulsion Lab. A mixture of the mineral in HPLC-grade water was stirred with a magnetic stirrer for 30 min to make a slurry of suspended minerals in water. Because the nebulizer utilizes vibrating mesh technology, to prevent the mesh from becoming clogged with mineral particles, the largest particles were settled out of solution before use. Settling velocities (w (cm/s)) of mineral particles in water were calculated based on Stokes' law

$$w = \frac{2(\rho_p - \rho_w)gr^2}{9\mu}$$

Here, ρ_p and ρ_w are the bulk densities (g/cm^3) of the mineral particle and water, respectively, g is the acceleration of gravity (9.8 m/s^2), r is the particle radius (cm), and μ is the dynamic viscosity of water (Pa·s). Densities of 2.2 and 2.9 g/cm^3 were used for montmorillonite and MMS, respectively. Values of density and viscosity for water at 20 °C were 0.998 g/cm^3 and 1.002 Pa·s, respectively. Particles larger than 1 μm in diameter settle out of a 3 cm column in 13 and 8 h for montmorillonite and MMS, respectively. The particle size distribution of the resulting stream of soluble and insoluble heterogeneous nuclei was measured using a scanning mobility particle sizer (SMPS TSI model 3010). The average size distributions from three samples from each of the heterogeneous nuclei types are shown in Figure S1 of the Supporting Information. The mode diameters of the heterogeneous nuclei ranged from 200 to 400 nm.

3.4. Imaging Efflorescence and Collisions. To monitor collisions between the levitated droplet and heterogeneous nuclei and to detect efflorescence, two charge-coupled device (CCD) cameras are placed outside the windows of the flow cell, oriented perpendicular to the laser axis. Far-field scattering of the trapping laser as well as the bright-field image taken by adding an LED light source is captured by the cameras. The two CCDs are controlled with a LabView program that records, stores, and replays video files. When observed in far

https://dx.doi.org/10.1021/acsearthspacechem.0c00161
ACS Earth Space Chem. 2020, 4, 1947−1956

field, the light scattering is used to determine the phase state of the levitated droplet. As seen in Figure 1, when the levitated

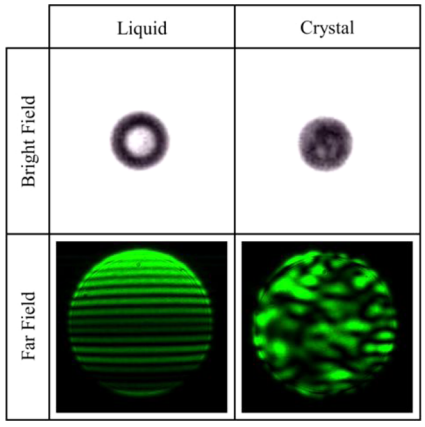

Figure 1. Images of $Mg(ClO_4)_2$ liquid droplet and crystal in bright field and far field. Brightness and contrast of the bright-field images have been increased to better distinguish the two images.

droplet is liquid, a Mie scattering pattern with alternating bright and dark bands occurs. The relative intensity and spacing of the bands depend on the size and refractive index of the droplet and change as RH changes. Larger particles have closer band spacings than smaller particles. Once the droplet has effloresced and become crystalline, the alternating bands disappear, and the scattering pattern becomes mosaic. As discussed in previous studies with the optical levitator, the loss of the linear Mie scattering pattern is consistent with crystallization.[25,26] Further, as the trapped crystal constantly rotates in the trap, the scattering pattern changes with time as different crystal faces interact with the laser. Bright-field images of the crystal can also sometimes be used to determine efflorescence. As seen in Figure 1, the liquid droplet appears round and homogeneous. In contrast, while the overall shape of this particular crystalline particle is spherical, inhomogeneities due to light passing through the crystal facets are observed.

The cameras are also used to identify collisions between the trapped droplet and the incoming heterogeneous nucleus. While there are several ways to determine whether a collision occurs in the trap, here we show an example that only uses far-field imaging. Figure 2 shows an experiment where a droplet of $Mg(ClO_4)_2$ comes into contact with two different heterogeneous nuclei, crystalline $Mg(ClO_4)_2$ and NaCl, at a similar RH but with different outcomes. In panel A, crystalline $Mg(ClO_4)_2$ comes in from below and collides with the droplet inducing immediate efflorescence, as indicated by the change in the light scattering pattern. As the effloresced particle is stabilized in the trap, it rises in the trap at a higher position as a result of losing water and thus mass. The rise in the trapping position is also used as an additional indicator of efflorescence. In panel B, a crystal of NaCl collides with the droplet of $Mg(ClO_4)_2$, but unlike the previous experiment, it does not cause efflorescence. The crystal becomes immersed into the droplet and dissolves away without changing the light scattering or the trapping position. The diffused light coming from the bottom is the light scattered off the heterogeneous nucleus. The scattered light from the heterogeneous nucleus and levitated droplet appear to be the same size because we are observing in the far field and the scattered images are cut off by the windows on

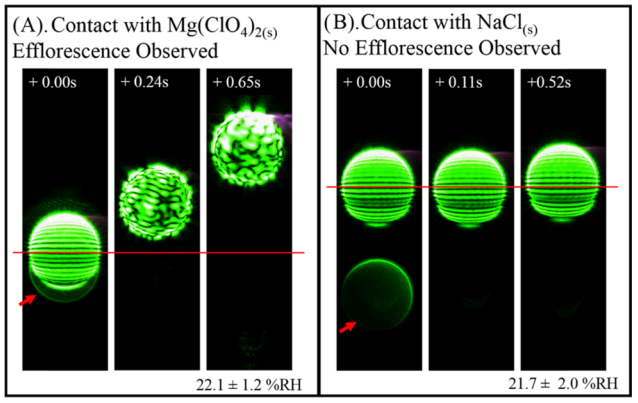

Figure 2. Sequence of images from a contact efflorescence experiment of $Mg(ClO_4)_2$ by a crystal of (A) $Mg(ClO_4)_2$ and (B) NaCl. Both experiments were conducted at approximately 22% RH. The red solid line is a reference for the vertical position of the droplet. The red arrows on the first frames point to the heterogeneous nucleus.

the flow cell. The circular windows cut off the scattered light; thus, all of the far-field images are circular and of the same size due to the window. However, the small heterogeneous nucleus has only one apparent band, while the large droplet has a scattering pattern with many bands.

3.5. Determining Contact and Immersion Heterogeneous ERH. Two separate experimental methods were utilized to determine contact and immersion ERH. For contact efflorescence, droplets of the brine were trapped at an RH between the homogeneous ERH and DRH. Each trial consisted of exposing the trapped droplet to a stream of the dried heterogeneous nucleus for either 25 s for the soluble salts or 60 s for the insoluble mineral particles at a constant RH. The difference in exposure time was due to the difference in collision rates between insoluble and soluble heterogeneous nuclei, possibly arising from the different methods used to create nebulized particles. The soluble heterogeneous nuclei on average would collide with the trapped droplet every 4.2 ± 1.8 s, while the insoluble mineral particles would collide every 9.5 ± 1.6 s. Thus, the trapped droplet would be exposed to approximately six collisions totally per trial for both insoluble and soluble heterogeneous nuclei. However, the number of collisions may be an underestimate as heterogeneous nuclei scatter less light as their size decreases. Thus, a heterogeneous nucleus that is too small may not scatter ample light to be observed on the CCD camera. The droplet was monitored for whether it effloresced during the exposure period. If the droplet did not effloresce, then the droplet was ejected from the trap and a new droplet was trapped for the next trial. The process was repeated to calculate a probability of efflorescence (P_{eff}) as the ratio of the observed efflorescence events to the number trials as a function of RH. Contact ERH was then reported as the RH, where P_{eff} was equal to 0.5.

For immersion efflorescence, a droplet of the brine at an RH significantly higher than homogeneous ERH and the contact ERH was exposed to a stream of heterogeneous nuclei. The humid conditions ensured that the droplet did not undergo contact efflorescence during the process of immersing the mineral particle into the brine. The droplet was monitored until a collision with a mineral particle was visually observed and was then isolated from further collisions by adjusting the slidable mount to direct the particles away from the droplet. A video recording from the CCDs was reviewed to confirm a

https://dx.doi.org/10.1021/acsearthspacechem.0c00161
ACS Earth Space Chem. 2020, 4, 1947−1956

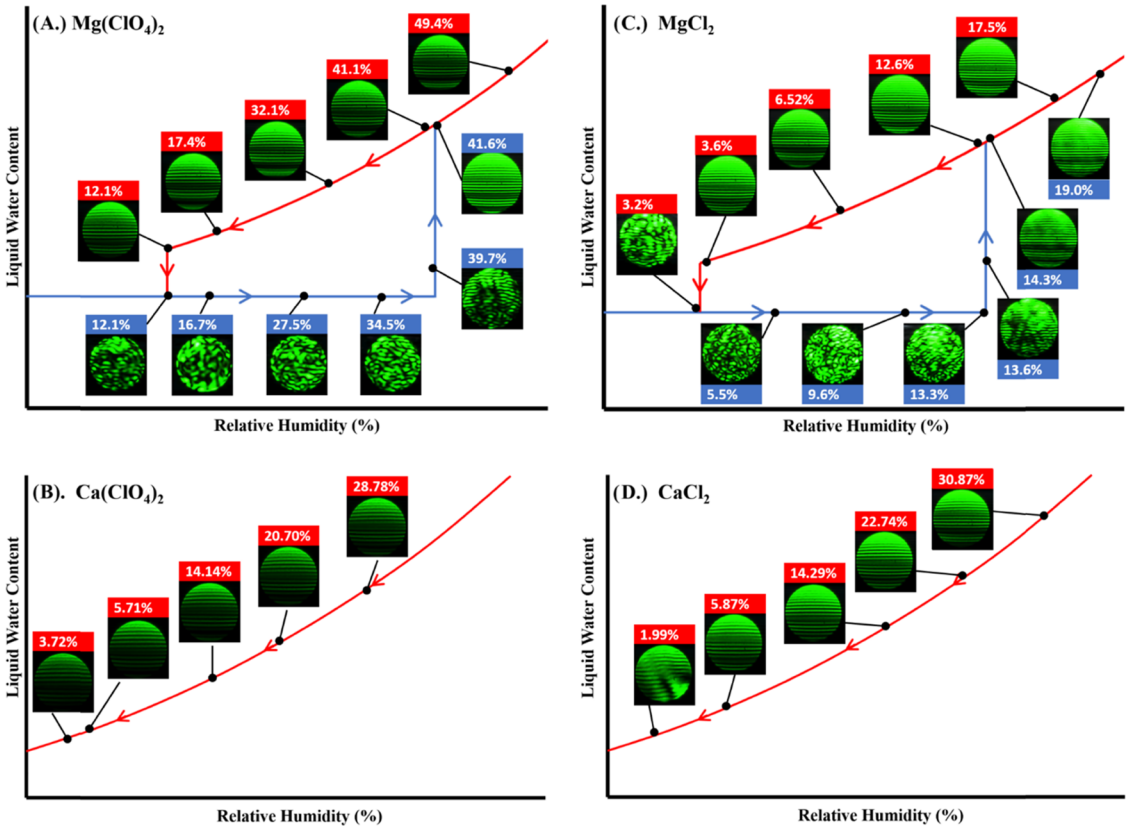

Figure 3. Homogeneous hysteresis of (A) $Mg(ClO_4)_2$, (B) $Ca(ClO_4)_2$, (C) $MgCl_2$, and (D) $CaCl_2$. The red line indicates dehumidification, and the blue line indicates humidification. Scattering images in the far field are shown for various humidities along hysteresis. The liquid water content and relative humidity are not to scale.

collision. If multiple collisions were observed, the number of collisions was kept to a maximum of three. Droplets with more than three collisions were expelled from the trap and a new droplet was caught. The RH inside the flow cell was then lowered at a rate of ≤1% RH/min until efflorescence occurred. Immersion ERH was reported as the average RH (±1 S.D.) of all of the RH values where immersion efflorescence was observed.

4. RESULTS

4.1. Homogeneous Efflorescence of Brines. Examples of the homogeneous phase transition of all four salts at room temperature are shown in Figure 3. In Figure 3A, we begin with a droplet of aqueous $Mg(ClO_4)_2$ at a humidity of 49.4% RH at the top right of the panel along the red curve. As the humidity is lowered, the droplet slowly loses water but remains a liquid as seen by the scattering pattern. The change in size due to loss of water is also seen through the changes to the Mie scattering peaks. At 12.1% RH, the droplet effloresces, signified by the abrupt change in scattering pattern shown by two images taken immediately before and after efflorescence. The trapped crystal is subsequently humidified (blue line), but the scattering pattern does not change until 39.7% RH when the Mie scattering returns, signifying a deliquescence event. The average homogeneous ERH and DRH values for $Mg(ClO_4)_2$ across all experiments conducted were 13.0 ± 0.5 and 39.7 ± 0.7% RH, respectively.

In contrast to $Mg(ClO_4)_2$, homogeneous efflorescence of $Ca(ClO_4)_2$ was not observed even when dried down to a humidity of 3.1% RH. This is shown in Figure 3B where a droplet of $Ca(ClO_4)_2$ begins at a humidity of 28.8% RH and is dried along the red curve. As RH is lowered, the $Ca(ClO_4)_2$ droplet loses water as seen in the changes in Mie scattering, similar to $Mg(ClO_4)_2$. However, as the humidity begins to reach the low single digits, the linear Mie scattering pattern remains indicating that the droplet has not effloresced. In all experiments conducted, dehumidification of $Ca(ClO_4)_2$ in our optical trap did not cause efflorescence. This study cannot rule out efflorescence occurring below 3.1% RH. However, a previous study that examined $Ca(ClO_4)_2$ showed that the brine did not homogeneously effloresce at RH <1% at room temperature.[13]

The homogeneous phase transition of droplets of $MgCl_2$ and $CaCl_2$ is shown in Figure 3C,D, respectively. On average, $MgCl_2$ undergoes efflorescence and deliquescence at 3.7 ± 0.4 and 13.7 ± 0.5% RH, respectively. Similar to $Ca(ClO_4)_2$, $CaCl_2$ does not homogeneously effloresce when dried and thus the DRH could not be measured. However, at low RH, interferences in the scattering pattern appear, which could indicate changes to the morphology of the droplet or localized changes in the refractive index of the droplet. For our study, the homogeneous DRH value at room temperature was estimated to be 15% RH based on a study that utilizes the droplet on a plate technique coupled with Raman microscopy.[16]

4.2. Heterogeneous Efflorescence of Brines. The probability of efflorescence for $Mg(ClO_4)_2$ in contact with the various heterogeneous nuclei is shown in Figure 4. The P_{eff} for each heterogeneous nucleus, with the exception of MMS, was fit with a sigmoidal curve that was bound between 0 and 1.

https://dx.doi.org/10.1021/acsearthspacechem.0c00161
ACS Earth Space Chem. 2020, 4, 1947−1956

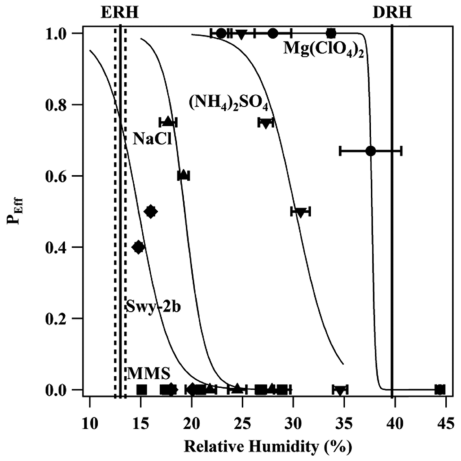

Figure 4. Contact efflorescence experiment results for $Mg(ClO_4)_2$ in contact with $Mg(ClO_4)_2$ (solid circle), $(NH_4)_2SO_4$ (solid down triangle), NaCl (solid up triangle), Na-montmorillonite (solid diamond), and MMS (solid square). Each was fitted with a sigmoidal curve. The two solid lines show the homogeneous ERH and DRH values for $Mg(ClO_4)_2$. The two dashed lines around the ERH line indicate the standard deviation in the homogeneous ERH as observed in this study.

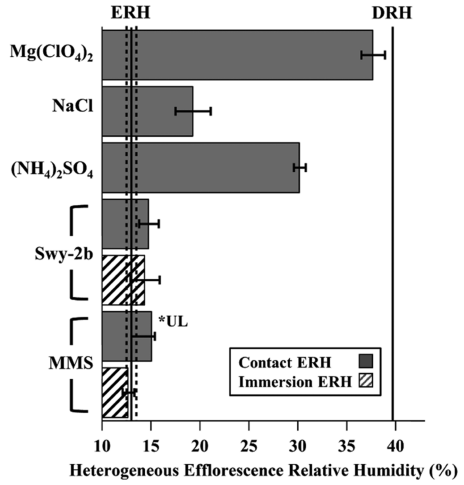

Figure 5. Summary of results for heterogeneous efflorescence of $Mg(ClO_4)_2$, NaCl, $(NH_4)_2SO_4$, Na-montmorillonite (Swy-2b), and MMS. The solid boxes indicate contact ERH, and the hatched boxes indicate immersion ERH. The two solid lines show the homogeneous ERH and DRH values for $Mg(ClO_4)_2$. The two dashed lines around the ERH line indicate the standard deviation in the homogeneous ERH as observed in this study. The *UL indicates that the value shown is the upper limit as contact efflorescence was never observed.

From the fitted curves, the half-max value (P_{eff} = 0.5) with a 90% confidence band was reported as the contact ERH. Heterogeneous nuclei that are efficient at inducing efflorescence of $Mg(ClO_4)_2$ will have a higher contact ERH closer to the homogeneous DRH of 39.7% RH; thus, the contact efflorescence efficiency increases for the curves from left to right on the figure. From Figure 4, it can be seen that a crystal of $Mg(ClO_4)_2$ is the most effective heterogeneous nucleus. Because the crystal has an identical lattice structure to the nucleating material, crystalline $Mg(ClO_4)_2$ simply acts as a seed for further crystallization and thus it is not surprising that it is the most effective heterogeneous nucleus causing efflorescence at 37.7 ± 1.2% RH. Since the contact ERH is close to the homogeneous DRH, a crystal of $Mg(ClO_4)_2$ will prevent any supersaturation of $Mg(ClO_4)_2$ brine it contacts. The next two most effective heterogeneous nuclei were $(NH_4)_2SO_4$ and NaCl with a contact ERH of 30.2 ± 0.6 and 19.3 ± 1.8% RH, respectively. The least effective heterogeneous nuclei were Na-montmorillonite and MMS. Na-montmorillonite induced contact efflorescence at 14.8 ± 1.0% RH, while MMS never induced efflorescence at the RH tested. Thus, an upper limit for contact ERH of $Mg(ClO_4)_2$ by MMS was chosen as the average RH (±1 S.D.) of the lowest set of RH tested at 15.1 ± 0.3% RH. When compared to the homogeneous ERH of $Mg(ClO_4)_2$ at 13.0% RH, neither Na-montmorillonite nor MMS seems to significantly increase the ERH of $Mg(ClO_4)_2$.

A summary of the results for all heterogeneous efflorescence experiments for $Mg(ClO_4)_2$ is shown in Figure 5. In addition to the contact ERH values, the immersion efflorescence values are also included for the nonsoluble heterogeneous nuclei. For Na-montmorillonite, the immersion ERH was 14.4 ± 1.5% RH, and for MMS, it was 12.7 ± 0.6% RH. As seen in the figure, Na-montmorillonite seems to have minimal effect on the efflorescence of $Mg(ClO_4)_2$ with both contact and immersion ERH not statistically different from the homogeneous ERH. Similarly, for MMS, the contact ERH is shown as an upper limit that is already close to the homogeneous ERH. Immersion efflorescence of $Mg(ClO_4)_2$ by MMS occurs at the homogeneous ERH within uncertainty. Thus, we conclude that at room temperature neither of these Mars soil analogues has a significant effect on the efflorescence of $Mg(ClO_4)_2$. The inactivity of the two insoluble Mars soil analogues as heterogeneous immersion nuclei for $Mg(ClO_4)_2$ was previously shown in a study performed on droplets on a plate at lower temperatures.[17] The contact and immersion ERH for Na-montmorillonite with $Mg(ClO_4)_2$ were the same, within error, unlike other studies that have found contact efflorescence to be more effective than immersion.[27] Here, neither contact nor immersion nucleation was effective.

The results for heterogeneous efflorescence of the remaining three brines $MgCl_2$, $Ca(ClO_4)_2$, and $CaCl_2$ by contact and immersion with Na-montmorillonite are shown in Figure 6. The contact ERH of $MgCl_2$ at 10.9 ± 0.6% RH was reported in a previous study performed in our optical levitator,[27] and the immersion ERH at 7.9 ± 2.7% RH is from the current study. Unlike $Mg(ClO_4)_2$, the efflorescence of $MgCl_2$ is significantly influenced by the presence of Na-montmorillonite in both contact and immersion modes. Additionally, contact efflorescence of $MgCl_2$ by Na-montmorillonite occurs at a higher RH than immersion efflorescence. For the two calcium salts, since homogeneous deliquescence was not observed, the DRH value shown was taken from the literature.[13,16] Contact efflorescence experimental results for $Ca(ClO_4)_2$ and $CaCl_2$ are shown in Figure S2 of the Supporting Information. As seen in the figure, contact efflorescence of $Ca(ClO_4)_2$ and $CaCl_2$ by Na-montmorillonite was not observed. The lowest average RH values achieved for $Ca(ClO_4)_2$ and $CaCl_2$ were 5.2 ± 0.5 and 4.9 ± 0.6% RH, respectively. Thus, these values also represent upper limits for contact ERH. Similarly, immersion efflorescence was not observed for the two calcium salts by Na-montmorillonite. The average of the five lowest RH values reached in immersion experiments for $Ca(ClO_4)_2$ and $CaCl_2$ were 3.1 ± 0.9 and 2.7 ± 0.3% RH, respectively. Thus, these values represent the upper limits for immersion ERH.

https://dx.doi.org/10.1021/acsearthspacechem.0c00161
ACS Earth Space Chem. 2020, 4, 1947−1956

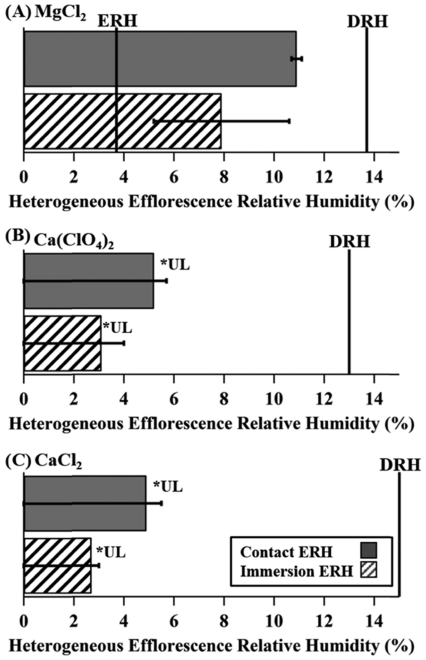

Figure 6. Summary of results for heterogeneous efflorescence experiments of (A) $MgCl_2$, (B) $Ca(ClO_4)_2$, and (C) $CaCl_2$ by Na-montmorillonite. The solid boxes are for contact ERH values, while the hatched boxes are for immersion ERH values. The solid lines indicate the homogeneous ERH and DRH values for each salt. DRH values for $Ca(ClO_4)_2$[13] and $CaCl_2$[16] were taken from the literature. *UL represents an upper limit as heterogeneous efflorescence was never observed in those experiments.

However, it is still possible for contact and immersion efflorescence to occur at RH values below the reported values.

5. DISCUSSION

5.1. Heterogeneous Efflorescence on Mars. Comparisons of the homogeneous phase diagrams for the four magnesium and calcium salts to temperature and humidity conditions on Mars have shown that some salt brines on Mars may be stable for certain periods of time during a Martian sol.[10−14] When the homogeneous phase transitions of $Mg(ClO_4)_2$ are compared to modeled surface temperature and humidity conditions at the Viking Lander 2 site, $Mg(ClO_4)_2$ does not seem to deliquesce for any significant amount of time.[10] However, when the same diurnal trajectory is compared to the stability phase diagram of $Ca(ClO_4)_2$, brine could be stable or metastable for 3−4 h per sol.[13] Additionally, the temperature and humidity conditions of the shallow subsurface were modeled at the Phoenix landing site, and when that trajectory is applied to the stability diagram of $Ca(ClO_4)_2$, it was shown that the stability period could be as long as 17 h.[13] The modeled shallow subsurface was significantly warmer and more humid, never dropping below 8% RH, which allowed the brine to be stable for a longer time. Since the homogeneous ERH of $Mg(ClO_4)_2$ is above 8% RH, efflorescence is likely to occur even in the subsurface. In contrast, $MgCl_2$, $Ca(ClO_4)_2$, and $CaCl_2$ have a lower homogeneous ERH, allowing them to possibly avoid efflorescence and persist as metastable, supersaturated brines. These studies did not, however, consider the possibility of heterogeneous nucleation of the briny droplets by contact or immersion of Martian regolith materials. Our studies show that Na-montmorillonite can act as a heterogeneous nucleus for the efflorescence of $MgCl_2$, increasing the heterogeneous ERH to 10.9 and 7.9% for contact and immersion ERH, respectively. The presence of montmorillonite could thus cause $MgCl_2$ to effloresce in the shallow subsurface, cutting into the stability period of $MgCl_2$ brine. For the two calcium salts, the inactivity of montmorillonite as a heterogeneous nucleus confirms the current expectation that their brines are metastable in the subsurface of Mars as the reported upper limits for heterogeneous ERH were not above 8%.

While the current study was conducted at room temperature, the average temperature of Mars is 210 K. During the warmer months on Mars, the temperatures can reach up to 300 K at equatorial regions,[7] but those high temperatures are accompanied by low RH values. Thus, the question arises as to the relevance of these results for Mars. However, past work has shown that homogeneous efflorescence is less dependent on temperature than deliquescence for these salts.[10−14] For example, Gough et al.[10] examined the homogeneous efflorescence of $Mg(ClO_4)_2$ and found minimal temperature dependence over the temperature range of 223−270 K. Further, a study by Primm et al.[17] over a similar temperature range examined immersion efflorescence of $Mg(ClO_4)_2$ by montmorillonite and MMS and again saw that efflorescence was independent of temperature. Thus, we expect a minimal temperature dependence for contact efflorescence as well, although this has not been proven.

5.2. Crystal Lattice Match. The effectiveness of foreign nuclei on crystal nucleation is often discussed in terms of the crystal lattice match between the two solids. It is believed that when a heterogeneous nucleus has a similar crystal lattice structure to the nucleating crystal, it will be more effective than the one that lacks a crystal lattice match.[40,41] For efflorescence, a better crystal match would induce efflorescence at a relative humidity closer to the homogeneous DRH,[26,27] thus preventing brine supersaturation. To compare the various heterogeneous nuclei's crystal lattice to that of the effloresced crystal from the brine, the crystal lattice mismatch (δ) between their crystal faces was calculated

$$\delta = \frac{\left|\frac{a_{1,\mathrm{HN}} - a_{1,\mathrm{Cr}}}{a_{1,\mathrm{Cr}}}\right| + \left|\frac{a_{2,\mathrm{HN}} - a_{2,\mathrm{Cr}}}{a_{2,\mathrm{Cr}}}\right|}{2}$$

Here, a_1 and a_2 are the two lattice constants that define the specific crystal face for the heterogeneous nucleus (HN) and the nucleating crystal (Cr). A crystal lattice mismatch of zero means a perfect match, as the value for crystal lattice mismatch increases, the more dissimilar the two crystal systems are. A crystal lattice was simplified to the three faces: the 100 face is represented by the b and c lattice constants, the 010 by the c and a, and the 001 by the a and b lattice constants. Each of these faces of the brine crystal was compared to that of the heterogeneous nuclei, resulting in a total of nine calculated crystal lattice mismatches for each pair. Of the nine calculated values, the lowest value was determined as the crystal lattice mismatch. The crystal lattice mismatch between $Mg(ClO_4)_2$ and four of the heterogeneous nuclei ($Mg(ClO_4)_2$, $(NH_4)_2SO_4$, NaCl, and Na-montmorillonite) was calculated and compared to their respective contact ERH in Figure 7. MMS was excluded from this analysis because it is a mixture of minerals. The data was fit with a linear fit, and the resulting R-squared value is shown. A list of the lattice constants and

https://dx.doi.org/10.1021/acsearthspacechem.0c00161
ACS Earth Space Chem. 2020, 4, 1947−1956

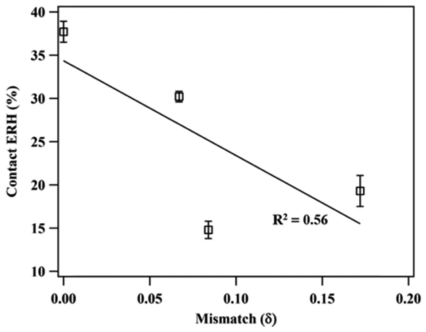

Figure 7. Contact ERH of $Mg(ClO_4)_2$ compared to lattice mismatch (δ) with linear fit and *R*-squared values.

crystal systems of the species analyzed are shown in Table S1 of the Supporting Information. There is a mild negative correlation between contact ERH and lattice mismatch, implying that a heterogeneous nucleus with a more similar crystal lattice to the brine tends to be more effective at inducing contact mode efflorescence. The result is as expected and is also consistent with previous studies on heterogeneous efflorescence in the optical trap.[26,27] Those studies found that when the lattice mismatch value was above 0.12, the heterogeneous nuclei were typically not effective at inducing contact efflorescence of the nucleating salt.

To predict the global effect of heterogeneous nuclei on brine stability, the crystal lattice mismatch between $Mg(ClO_4)_2$, $MgCl_2$, $Ca(ClO_4)_2$, and $CaCl_2$ and a set of minerals that have been detected either remotely or in situ were calculated and are tabulated in Table 1. The mismatch values were then designated a color based on the predicted effectiveness of the mineral in inducing efflorescence. Green ($\delta < 0.06$) represents pairings where the heterogeneous nucleus is likely to impact brine stability, yellow ($0.06 < \delta < 0.12$) represents minerals that may or may not impact the brine, and red ($0.12 < \delta$) is unlikely to have an impact. As shown in the table, most of the brine and mineral pairings have a lattice mismatch above 0.12. Many of the clay minerals such as nontronite and montmorillonite have a lattice mismatch that is between 0.06 and 0.12 for the salts except for $CaCl_2$. Additionally, of the four salts, $MgCl_2$ has the lowest mismatch value with montmorillonite, which could explain why $MgCl_2$ was the only brine whose stability was significantly decreased by montmorillonite. There are only four pairings that have a mismatch value below 0.06 with two of them being for contact with $Mg(ClO_4)_2$. At the surface of Mars, $Mg(ClO_4)_2$ is already thought to not undergo deliquescence. However, in the shallow subsurface where $Mg(ClO_4)_2$ may transition into brine for short periods of time, the presence of hematite and chlorite may limit brine metastability. Kieserite ($MgSO_4$), which has been detected by the Opportunity rover and has been theorized to have an association with groundwater upwelling events,[33] has a low mismatch value for $CaCl_2$. Feldspar contacting $MgCl_2$ is the final pair to have a mismatch value below 0.06 and is also the lowest mismatch value calculated from the selected list. Additionally, feldspar is the only mineral from the selected list that does not have a mismatch value above 0.12 with the four brines. As feldspar is believed to be globally distributed on Mars, its effect on brine stability may have the most impact.

6. CONCLUSIONS

On the surface of Mars, if droplets of a deliquesced salt were to form, they will likely interact with a heterogeneous nucleus such as other crystalline salts and mineral particles. Whether the heterogeneous nucleus will destabilize the brine and induce efflorescence at a significantly higher humidity than previously believed is dependent upon the combination of the aqueous salt and the nucleus. Some combinations, such as a crystalline $Mg(ClO_4)_2$ with a brine of itself or Na-montmorillonite with $MgCl_2$ brine, can significantly lower the stability of the aqueous solution and will lower the probability or duration of brines on

Table 1. Crystal Lattice Mismatch of Select Brines and Mineral Pairs

	$Mg(ClO_4)_2 \bullet 6H_2O$	$MgCl_2 \bullet 4H_2O$	$Ca(ClO_4)_2 \bullet 4H_2O$	$CaCl_2 \bullet 6H_2O$
Olivine	0.188	0.122	0.102	0.225
Orthopyroxene	0.175	0.237	0.14	0.226
Clinopyroxene	0.134	0.17	0.131	0.187
Feldspar	0.07	0.01	0.105	0.08
Hematite	0.032	0.277	0.136	0.318
Nontronite	0.088	0.099	0.097	0.201
Montmorillonite	0.084	0.08	0.099	0.199
Kaolinite	0.085	0.098	0.1	0.189
Chlorite	0.039	0.181	0.103	0.248
Illite	0.086	0.065	0.082	0.218
Prehnite	0.207	0.355	0.228	0.24
Quartz	0.186	0.336	0.195	0.279
Magnesite	0.117	0.361	0.227	0.292
Calcite	0.159	0.36	0.228	0.315
Kieserite	0.164	0.072	0.142	0.031
Gypsum	0.176	0.216	0.23	0.228

https://dx.doi.org/10.1021/acsearthspacechem.0c00161
ACS Earth Space Chem. 2020, 4, 1947−1956

Mars. However, other combinations such as MMS with $Mg(ClO_4)_2$ and Na-montmorillonite with $Mg(ClO_4)_2$, $Ca(ClO_4)_2$, and $CaCl_2$ did not impact the efflorescence when compared to homogeneous efflorescence. For the two calcium salts studied, the inactivity of montmorillonite as a heterogeneous nucleus is promising for liquid water on Mars as these salts are theorized to be in the brine form for extended periods of time on Mars.[13,14] However, to fully understand efflorescence and deliquescence on Mars' surface and subsurface, a model for heterogeneous efflorescence is necessary as it is impractical to study every possible combination of brine or mineral in the laboratory. This work shows that crystal lattice is one factor that determines how effective a heterogeneous nucleus will be in inducing efflorescence, but crystal lattice is one of the many factors believed to drive heterogeneous nucleation. For example, the number of active sites is also believed to affect heterogeneous nucleation.[28,29,42] Active sites are regions on a particle's surface where nucleation is most likely to begin, believed to be formed from defects to the mineral's structure. Studies that have examined the size effect of immersed metal oxide particles on efflorescence of $(NH_4)_2SO_4$ have suggested that by increasing the surface area, the number of active sites were increased and thus a higher immersion ERH was observed.[28,29] For an accurate model of heterogeneous efflorescence, additional laboratory studies that probe and parameterize the many factors of heterogeneous nucleation will need to be conducted.

■ ASSOCIATED CONTENT

Supporting Information

The Supporting Information is available free of charge at https://pubs.acs.org/doi/10.1021/acsearthspacechem.0c00161.

Plots of particle size distributions for all heterogeneous nuclei used in the study (Figure S1); contact efflorescence experiment results for $Ca(ClO_4)_2$ and $CaCl_2$ (Figure S2); and table of lattice constants and crystal systems for all salts and mineral particles analyzed (Table S1) (PDF)

■ AUTHOR INFORMATION

Corresponding Author

Margaret A. Tolbert − *Department of Chemistry, University of Colorado Boulder, Boulder, Colorado 80309, United States; Cooperative Institute for Research in Environmental Science, Boulder, Colorado 80309, United States;* orcid.org/0000-0001-5730-6412; Phone: (303) 492-3179; Email: margaret.tolbert@colorado.edu

Authors

Shuichi B. Ushijima − *Department of Chemistry, University of Colorado Boulder, Boulder, Colorado 80309, United States; Cooperative Institute for Research in Environmental Science, Boulder, Colorado 80309, United States;* orcid.org/0000-0002-9536-2295

Raina V. Gough − *Department of Chemistry, University of Colorado Boulder, Boulder, Colorado 80309, United States; Cooperative Institute for Research in Environmental Science, Boulder, Colorado 80309, United States;* orcid.org/0000-0003-2755-7282

Complete contact information is available at: https://pubs.acs.org/10.1021/acsearthspacechem.0c00161

Notes

The authors declare no competing financial interest.

■ ACKNOWLEDGMENTS

This material is based upon the work supported by the National Science Foundation under Grant No. AGS1925191, and this work was supported by NASA Headquarters under the NASA Earth and Space Science Fellowship Program, Grant "80NSSC17K0655".

■ REFERENCES

(1) Cockell, C. S.; Bush, T.; Bryce, C.; Direito, S.; Fox-Powell, M.; Harrison, J. P.; Lammer, H.; Landenmark, H.; Martin-Torres, J.; Nicholson, N.; Noack, L.; O'Malley-James, J.; Payler, S. J.; Rushby, A.; Samuels, T.; Schwendner, P.; Wadsworth, J.; Zorzano, M. P. Habitability: A Review. *Astrobiology* **2016**, *16*, 89−117.

(2) Ehlmann, B. L.; Anderson, F. S.; Andrews-Hanna, J.; Catling, D. C.; Christensen, P. R.; Cohen, B. A.; Dressing, C. D.; Edwards, C. S.; Elkins-Tanton, L. T.; Farley, K. A.; Fassett, C. I.; Fischer, W. W.; Fraeman, A. A.; Golombek, M. P.; Hamilton, V. E.; Hayes, A. G.; Herd, C. D. K.; Horgan, B.; Hu, R.; Jakosky, B. M.; Johnson, J. R.; Kasting, J. F.; Kerber, L.; Kinch, K. M.; Kite, E. S.; Knutson, H. A.; Lunine, J. I.; Mahaffy, P. R.; Mangold, N.; McCubbin, F. M.; Mustard, J. F.; Niles, P. B.; Quantin-Nataf, C.; Rice, M. S.; Stack, K. M.; Stevenson, D. J.; Stewart, S. T.; Toplis, M. J.; Usui, T.; Weiss, B. P.; Werner, S. C.; Wordsworth, R. D.; Wray, J. J.; Yingst, R. A.; Yung, Y. L.; Zahnle, K. J. The Sustainability of Habitability on Terrestrial Planets, Insights, Question, and Needed Measurements from Mars for Understanding the Evolution of Earth-like Worlds. *J. Geophys. Res.: Planets* **2016**, *121*, 1927−1961.

(3) Mangold, N.; Quantin, C.; Ansan, V.; Delacourt, C.; Allemand, P. Evidence for Precipitation on Mars from Dendritic Valleys in the Valles Marineris Area. *Science* **2004**, *305*, 78−81.

(4) Bibring, J. P.; Langevin, Y.; Mustard, J. F.; Poulet, F.; Arvidson, R.; Gendrin, A.; Gondet, B.; Mangold, N.; Pinet, P.; Forget, F.; the OMEGA team; et al. Global Mineralogical and Aqueous Mars History Derived from OMEGA/Mars Express Data. *Science* **2006**, *312*, 400−404.

(5) Ehlmann, B. L.; Mustard, J. F.; Murchie, S. L.; Bibring, J. P.; Meunier, A.; Fraeman, A. A.; Langevin, Y. Subsurface Water and Clay Mineral Formation During the Early History of Mars. *Nature* **2011**, *479*, 53−60.

(6) Poulet, F.; Bibring, J.-P.; Mustart, J. F.; Gendrin, A.; Mangold, N.; Langevin, Y.; Arvidson, R. E.; Gondet, B.; Gomez, C.; the OMEGA Team. Phyllosilicates on Mars and Implications for Early Martian Climate. *Nature* **2005**, 623−627.

(7) McEwen, A. S.; Ojha, L.; Dundas, C. M.; Mattson, S. S.; Byrne, S.; Wray, J. J.; Cull, S. C.; Murchie, S. L.; Thomas, N.; Gulick, V. C. Season Flows on Warm Martian Slopes. *Science* **2011**, *333*, 740−743.

(8) Ojha, L.; Wilhelm, M. B.; Murchie, S. L.; McEwen, A. S.; Wray, J. J.; Hanley, J.; Masse, M.; Chojnacki, M. Spectral Evidence for Hydrated Salts in Recurring Slope Lineae on Mars. *Nat. Geosci.* **2015**, *8*, 829−832.

(9) Martin-Torres, F. J.; Zorzano, M. P.; Valenti'n-Serrano, P.; Harri, A. M.; Genzer, M.; Kemppinen, O.; Rivera-Valentin, E. G.; Jun, I.; Wray, J.; Madsen, M. B.; Goetz, W.; McEwen, A. S.; Hardgrove, C.; Renno, N.; Chevrier, V. F.; Mischna, M.; Navarro-Gonza'lez, R.; Marti'nez-Fri'as, J.; Conrad, P.; McConnochie, T.; Cockell, C.; Berger, G.; Vasavada, A. R.; Sumner, D.; Vaniman, D. Transient Liquid Water and Water Activity at Gale Crater on Mars. *Nat. Geosci.* **2015**, *8*, 357−361.

(10) Gough, R. V.; Chevrier, V. F.; Baustian, K. J.; Wise, M. E.; Tolbert, M. A. Laboratory Studies of Perchlorate Phase Transition: Support for Metastable Aqueous Perchlorate Solutions on Mars. *Earth Planet. Sci. Lett.* **2011**, *312*, 371−377.

(11) Nuding, D. L.; Davis, R. D.; Gough, R. V.; Tolbert, M. A. The Aqueous Stability of a Mars Salt Analog: Instant Mars. *J. Geophys. Res.: Planets* **2015**, *120*, 588−598.

(12) Primm, K. M.; Gough, R. V.; Chevrier, V. F.; Tolbert, M. A. Freezing of Perchlorate and Chloride Brines Under Mars-Relevant Conditions. *Geochim. Cosmochim. Acta* **2017**, *212*, 211−220.
(13) Nuding, D. L.; Rivera-Valentin, E. G.; Davis, R. D.; Gough, R. V.; Chevrier, V. F.; Tolbert, M. A. Deliquescence and Efflorescence of Calcium Perchlorate: An Investigation of Stable Aqueous Solutions Relevant to Mars. *Icarus* **2014**, *243*, 420−428.
(14) Gough, R. V.; Chevrier, V. F.; Tolbert, M. A. Formation of Aqueous Solutions on Mars via Deliquescence of Chloride-Perchlorate Binary Mixture. *Earth Planet. Sci. Lett.* **2014**, *393*, 73−82.
(15) Martínez, G. M.; Renno, N. O. Water and Brines on Mars: Current Evidence and Implications for MSL. *Space Sci. Rev.* **2013**, *175*, 29−51.
(16) Gough, R. V.; Chevrier, V. F.; Tolbert, M. A. Formation of Liquid Water at Low Temperature via the Deliquescence of Calcium Chloride: Implications for Antarctica and Mars. *Planet. Space Sci.* **2016**, *131*, 79−87.
(17) Primm, K. M.; Gough, R. V.; Wong, J.; Rivera-Valentin, E. G.; Martinez, G. M.; Hogancamp, J. V.; Archer, P. D.; Ming, D. W.; Tolbert, M. A. The Effect of Mars-Relevant Soil Analogs on the Water Uptake of Magnesium Perchlorate and Implications for the Near-Surface of Mars. *J. Geophys. Res.: Planets* **2018**, *123*, 2076−2088.
(18) Toner, J. D.; Catling, D. C.; Light, B. The Formation of Supercooled Brines, Viscous Liquids, and Low-Temperature Perchlorate Glasses in Aqueous Solutions Relevant to Mars. *Icarus* **2014**, *233*, 36−47.
(19) Zorzano, M.-P.; Mateo-Marti, E.; Prieto-Ballesteros, O.; Osuna, S.; Renno, N. Stability of Liquid Saline Water on Present Day Mars. *Geophys. Res. Lett.* **2009**, *36*, No. L20201.
(20) Hecht, M. H.; Kounaves, S. P.; Quinn, R. C.; West, S. J.; Young, S. M. M.; Ming, D. W.; Catling, D. C.; Clark, B. C.; Boynton, W. V.; Hoffman, J.; DeFlores, L. P.; Gospodinova, K.; Kapit, J.; Smith, P. H. Detection of Perchlorate and the Soluble Chemistry of Martian Soil at the Phoenix Lander Site. *Science* **2009**, *325*, 64−67.
(21) Glavin, D. P.; Freissinet, C.; Miller, K. E.; Eigenbrode, J. L.; Brunner, A. E.; Buch, A.; Sutter, B.; Archer, P. D., Jr.; Atreya, S. K.; Brinckerhoff, W. B.; Cabane, M.; Coll, P.; Conrad, P. G.; Coscia, D.; Dworkin, J. P.; Franz, H. B.; Grotzinger, J. P.; Leshin, L. A.; Martin, M. G.; McKay, C.; Ming, D. W.; Navarro-Gonza′lez, R.; Pavlov, A.; Steele, A.; Summons, R. E.; Szopa, C.; Teinturier, S.; Mahaffy, P. R. Evidence for Perchlorates and the Origin of Chlorinated Hydrocarbons Detected by SAM at the Rocknest Aeolian Deposit in Gale Crater. *J. Geophys. Res.: Planets* **2013**, *118*, 1955−1973.
(22) Ming, D. W.; Archer, P. D., Jr.; Glavin, D. P.; Eigenbrode, J. L.; Franz, H. B.; Sutter, B.; Brunner, A. E.; Stern, J. C.; Freissinet, C.; McAdam, A. C.; Mahaffy, P. R.; Cabane, M.; Coll, P.; Campbell, J. L.; Atreya, S. K.; Niles, P. B.; Bell, J. F., III; Bish, D. L.; Brinckerhoff, W. B.; Buch, A.; Conrad, P. G.; Des Marais, D. J.; Ehlmann, B. L.; Faire′n, A. G.; Farley, K.; Flesch, G. J.; Francois, P.; Gellert, R.; Grant, J. A.; Grotzinger, J. P.; Gupta, S.; Herkenhoff, K. E.; Hurowitz, J. A.; Leshin, L. A.; Lewis, K. W.; McLennan, S. W.; Miller, K. E.; Moersch, J.; Morris, R. V.; Navarro-Gonza′lez, R.; Pavlov, A. A.; Perrett, G. M.; Pradler, I.; Squyres, S. W.; Summons, R. E.; Steele, A.; Stolper, E. M.; Sumner, D. Y.; Szopa, C.; Teintrier, S.; Trainer, M. G.; Treiman, A. H.; Vaniman, D. T.; Vasavada, A. R.; Webster, C. R.; Wray, J. J.; Yingst, R. A.; MSL Science Team; et al. Volatile and Organic Compositions of Sedimentary Rocks in Yellowknife Bay, Gale Crater, Mars. *Science* **2014**, *343*, No. 1245267.
(23) Clark, B. C.; Kounaves, S. P. Evidence for the Distribution of Perchlorates on Mars. *Int. J. Astrobiol.* **2016**, *15*, 311−318.
(24) Orosei, R.; Lauro, S. E.; Pettinelli, E.; Cicchetti, A.; Coradini, M.; Cosciotti, B.; Di Paolo, F.; Flamini, E.; Mattei, E.; Pajola, M.; Soldovieri, F.; Cartacci, M.; Cassenti, F.; Frigeri, A.; Giuppi, S.; Martufi, R.; Masdea, A.; Mitri, G.; Nenna, C.; Noschese, R.; Restano, M.; Seu, R. Radar Evidence of Subglacial Liquid Water on Mars. *Science* **2018**, *361*, 490−493.
(25) Davis, R. D.; Lance, S.; Gordon, J. A.; Tolbert, M. A. Long Working-Distance Optical Trap for in Situ Analysis of Contact-Induced Phase Transformations. *Anal. Chem.* **2015**, *87*, 6186−6194.
(26) Davis, R. D.; Lance, S.; Gordon, J. A.; Ushijima, S. B.; Tolbert, M. A. Contact Efflorescence as a Pathway for Crystallization of Atmospherically Relevant Particles. *Proc. Natl. Acad. Sci. U.S.A.* **2015**, *112*, 15815−15820.
(27) Ushijima, S. B.; Davis, R. D.; Tolbert, M. A. Immersion and Contact Efflorescence Induced by Mineral Dust Particles. *J. Phys. Chem. A* **2018**, *122*, 1303−1311.
(28) Martin, S. T.; Han, J.; Hung, H. The Size Effect of Hematite and Corundum Inclusions on the Efflorescence Relative Humidities of Aqueous Ammonium Sulfate Particles. *Geophys. Res. Lett.* **2001**, *28*, 2601−2604.
(29) Han, J.; Hung, H.; Martin, S. T. Size Effect of Hematite and Corundum Inclusions on the Efflorescence Relative Humidities of Aqueous Ammonium Nitrate Particles. *J. Geophys. Res.* **2002**, *107*, AAC 3-1−AAC 3-9.
(30) Pant, A.; Parsons, M. T.; Bertram, A. K. Crystallization of Aqueous Ammonium Sulfate Particles Internally Mixed with Soot and Kaolinite: Crystallization Relative Humidities and Nucleation Rates. *J. Phys. Chem. A* **2006**, *110*, 8701−8709.
(31) Zuberi, B.; Bertram, A. K.; Cassa, C. A.; Molina, L. T.; Molina, M. J. Heterogeneous Nucleation of Ice in $(NH_4)_2SO_4$-H_2O Particles with Mineral Dust Immersion. *Geophys. Res. Lett.* **2002**, *29*, 142-1−142-4.
(32) Ladino Moreno, L. A.; Stetzer, O.; Lohmann, U. Contact Freezing: A Review of Experimental Studies. *Atmos. Chem. Phys.* **2013**, *13*, 9745−9769.
(33) Ehlmann, B. L.; Edwards, C. S. Mineralogy of the Martian Surface. *Annu. Rev. Earth Planet. Sci.* **2014**, *42*, 291−315.
(34) Bibing, J. P.; Langevin, Y.; Gendrin, A.; Gondet, B.; Poulet, F.; Berthe, M.; Soufflot, A.; Arvidson, R.; Mangold, N.; Mustard, J.; Drossart, P.; the OMEGA team. Mars Surface Diversity as Revealed by the OMEGA/MARS Express Observation. *Science* **2005**, *307*, 1576−1581.
(35) Blake, D.; Vaniman, D.; Achilles, C.; Anderson, R.; Bish, D.; Bristow, T.; Chen, C.; Chipera, S.; Crisp, J.; Des Marais, D.; Downs, R. T.; Farmer, J.; Feldman, S.; Fonda, M.; Gailhanou, M.; Ma, H.; Ming, D. W.; Morris, R. V.; Sarrazin, P.; Stolper, E.; Treiman, A.; Yen, A. Characterization and Calibration of the CheMin Mineralogical Instrument on Mars Science Laboratory. *Space Sci. Rev.* **2012**, *170*, 341−399.
(36) Vaniman, D. T.; Bish, D. L.; Ming, D. W.; Bristow, T. F.; Morris, R. V.; Blake, D. F.; Chipera, S. J.; Morrison, S. M.; Treiman, A. H.; Rampe, E. B.; Rice, M.; Achilles, C. N.; Grotzinger, J. P.; McLennan, S. M.; Williams, J.; Bell, J. F., III; Newsom, H. E.; Downs, R. T.; Maurice, S.; Sarrazin, P.; Yen, A. S.; Morookian, J. M.; Farmer, J. D.; Stack, K.; Milliken, R. E.; Ehlmann, B. L.; Sumner, D. Y.; Berger, G.; Crisp, J. A.; Hurowitz, J. A.; Anderson, R.; Des Marais, D. J.; Stolper, E. M.; Edgett, K. S.; Gupta, S.; Spanovich, N.; MSL Science Team; et al. Mineralogy of a Mudstone at Yellowknife Bay, Gale Crater, Mars. *Science* **2014**, *343*, No. 1243480.
(37) Peters, G. H.; Abbey, W.; Bearman, G. H.; Mungas, G. S.; Smith, J. A.; Anderson, R. C.; Douglas, S.; Beegle, L. W. Mojave Mars Simulant − Characterization of a new geologic Mars analog. *Icarus* **2008**, *197*, 470−479.
(38) Osterloo, M. M.; Anderson, F. S.; Hamilton, V. E.; Hynek, B. M. Geologic context of proposed chloride-bearing materials on Mars. *J. Geophys. Res.* **2010**, *115*, No. E10012.
(39) Garimella, S.; Huang, Y.-W.; Seewald, J. S.; Cziczo, D. J. Cloud Condensation Nucleus Activity Comparison of Dry- and Wet-Generated Mineral Dust Aerosol: the Significance of Soluble Material. *Atmos. Chem. Phys.* **2014**, *14*, 6003−6019.
(40) Van Meel, J. A.; Sear, R. P.; Frenkel, D. Design Principles for Broad-Spectrum Protein-Crystal Nucleants with Nanoscale Pits. *Phys. Rev. Lett.* **2010**, *105*, No. 205501.
(41) Mithen, J. P.; Sear, R. P. Computer Simulation of Epitaxial Nucleation of a Crystal on a Crystalline Surface. *J. Chem. Phys.* **2014**, *140*, No. 084504.
(42) Fletcher, N. H. Active Sites and Ice Crystal Nucleation. *J. Atmos. Sci.* **1969**, *26*, 1266−1271.

https://dx.doi.org/10.1021/acsearthspacechem.0c00161
ACS Earth Space Chem. 2020, 4, 1947−1956